PERGAMON

Computers & Geosciences 29 (2003) 949–960

COMPUTERS & GEOSCIENCES

www.elsevier.com/locate/cageo

Automatic interpretation of magnetic data based on Euler deconvolution with unprescribed structural index ☆

Daniela Gerovska[a,*], Marcos J. Araúzo-Bravo[b]

[a] *Laboratory of Geothermics, Department of Earth Resources Engineering, Kyushu University, Fukuoka 812-8581, Japan*
[b] *Department of Electromechanical Engineering, University of Burgos, Burgos 09006, Spain*

Received 15 October 2002; received in revised form 19 March 2003; accepted 25 March 2003

Abstract

A tool for fully automatic magnetic data interpretation, solving Euler's homogeneity equation with unprescribed structural index and for a linear background in each moving window, is presented here. The implemented Euler deconvolution algorithm is based on the properties of the differential similarity transformation, which decouples the coordinates and the structural index of the singular point and the parameters of the linear background field. Since the deconvolution algorithm resolves the singular point locations well, this allows the application of a two stage clustering technique, focusing the estimated singular point coordinates and structural indices, followed by a statistical analysis of the final solutions. The automatic technique was tested on simple and complex 3D model magnetic anomalies. Finally, the technique was applied to real magnetic anomaly data from the Burgas region and the adjoining Black Sea shelf of Bulgaria. The tool consists of two main functions, written in Matlab v.5.3, requiring Matlab's SPLINE and STATISTICS toolkits.

Keywords: Euler's homogeneity equation; Differential similarity transformation; Linearisation; Clustering; Linear background

1. Introduction

The Euler deconvolution technique for estimating the depth and the horizontal position of the magnetic sources is based on solving Euler's homogeneity equation

$$(x-x_0)\frac{\partial F}{\partial x}+(y-y_0)\frac{\partial F}{\partial y}+(z-z_0)\frac{\partial F}{\partial z}=-NF, \qquad (1)$$

where the homogeneous function F is the observed field at location (x,y,z), caused by a source at location (x_0,y_0,z_0), and N, denoted as the structural index, is a measure of the rate of change of the field with distance. The Euler deconvolution method belongs to a class of techniques referred to as "automatic" depth estimation methods. These techniques are designed to provide analysis of large amounts of data, as opposed to methods that are useful for more detailed analysis of isolated anomalies (Thompson, 1982). The method treats the field sources not as preconceived geological models but rather as consisting of elementary point sources with different falloff rate of the field with distance.

In the recently developed methods based on applying Euler's equation, a system of linear equations with the source coordinates as unknowns is devised and solved for the central point of a moving window along the measured data grid. In general, due to the interference of anomalies of closely located sources or regional fields, the measured field $F(P)$ at a point $P(x,y,z)$ in a window is considered to be a sum of the point source anomaly $A(P)$ and a background field $B(P)$

$$F(P)=A(P)+B(P). \qquad (2)$$

☆ Code on server at http://www.iamg.org/CGEditor/index.htm

*Corresponding author. Fax: +81-92-642-3614.
E-mail addresses: daniela@mine.kyushu-u.ac.jp (D. Gerovska), marara@dali.eis.uva.es (M.J. Araúzo-Bravo).

0098-3004/03/$ - see front matter © 2003 Elsevier Ltd. All rights reserved.
doi:10.1016/S0098-3004(03)00101-8

Different authors have used different approximation models of the background in a single window. In the first applications of Euler's equation for determining the depth to simple models from magnetic data (Hood, 1965; Ruddock et al., 1966), the presence of background influence was not considered. The assumption of no background in the data would allow simultaneous estimation of the singular point coordinates and the structural index, using a linear least squares method. But such a simplified approach to the problem would produce dispersed solutions since regional fields or constant offsets due to nearby anomalies are almost always present (Thompson, 1982). In order to overcome the dispersed solutions problem, Thompson (1982) approximated the background in the moving window with a constant, which is a zero order Taylor series approximation of the background function. This approach introduced a non-linear relation between the unknown constant background and the structural index, which made impossible the direct application of the linear least squares method. Thompson (1982) solved the problem in the 2D case, proposing to linearize the resulting form of the Euler's equation by prescribing the structural index, thus turning it into a tentative parameter. Reid et al. (1990) extended the method for the 3D case and the use of tentative values for the structural index became an accepted norm in the geophysical literature (Barbosa et al., 1999; Mushayandebvu et al., 2001). But the use of tentative values of the structural index deprived the technique of the possibility to be fully automated. The interpreter still had to make estimates for the coordinates and the constant background in a window for a range of tentative values of the structural index. This approach concentrated the efforts on the problem of choosing the correct structural index. The approach involving estimation of the best structural index value with the purpose of linearising Euler's equation makes the choice for the correct solution too complex in the case of data with singular points with different structural indices, as is usual in the real case. In this general case, with the standard method every anomaly has to be isolated from the total grid and the correct index and window size should be chosen, which makes the interpretation too subjective and time consuming.

A widely used acceptance criterion for evaluation of the quality of the solutions is based on the rule that the correct structural index produces the most focused image of the source locations (Thompson, 1982; Reid et al., 1990). Another criterion is based on achieving the lowest correlation between the estimated background for the whole grid and the measured field (Barbosa et al., 1999).

Barbosa et al. (1999) proved that even when background field is not present, the estimation of the horizontal coordinates of the source are independent of the assumed tentative value of the structural index, but the estimate of the source depth is dependent. The latter conclusion shows that the depth estimates are more sensitive to an imprecisely prescribed structural index. This drawback suggests that other methods for linearising Euler's equation, which do not prescribe the structural index but, conversely, estimate it, should be used.

Hsu (2002) suggested linearisation of Eq. (1) for the case of constant background through the use of the vertical derivative of the measured field, instead of the field itself. This implies that calculation of all second order partial field derivatives is also required. In that case one should pay attention to the amplification of the noise during numerical differentiation (Hsu, 2002).

Another more precise model of the background effect is its first order Taylor series approximation, resulting in a linear function

$$B(x, y, z) = b_0 + b_x x + b_y y + b_z z, \tag{3}$$

where the origin of the coordinate system is the window centre and the constant term b_0 is the value of $B(P)$ in that point. The background approximation with a linear function in a window is more realistic, especially in the case of closely located anomalies that interfere with each other. Stavrev (1997) proposed an algorithm for linearizing Euler's equation in the case of a linear background with unprescribed structural index, based on the theory of differential similarity transformations.

2. Method

In order to preserve the most attractive feature of the Euler deconvolution method, automatic interpretation of large amounts of data, we chose to implement the algorithm of Stavrev (1997) using unprescribed structural index, which allows simultaneous estimation of the coordinates and the structural indices of the singular points with the more precise approximation of the background as linear.

The algorithm is based on the properties of the differential similarity transformation (DST) (Stavrev, 1997). A similarity transformation in relation to a coordinates centre $O'(a, b, c)$ is a homotopic transformation with a scaling parameter $n > 0$, represented by the equations

$$\begin{aligned} x' &= a + (x - a)n, \\ y' &= b + (y - b)n, \\ z' &= c + (x - c)n. \end{aligned} \tag{4}$$

A differential similarity transformation represents the difference between the original field and the field after a similarity transformation with respect to a certain central point of similarity (CPS) O' and a coefficient

of similarity $n = -N$. The DSTs operator $S^{-N}[\cdot]_{O'}$, applied on a general function $f(P)$, is defined in Stavrev (1997) as

$$S^{-N}[f(P)]_{O'} = -Nf(P) - \mathbf{R}_{O'P}\nabla_P f(P) \quad (5)$$

where P is the observation point, $\mathbf{R}_{O'P}$ is a vector from a point O' to the point P, and $\nabla_P f(P)$ is the gradient of f with respect to P. In the case of a magnetic or gravity anomaly A, the distribution and amplitude of $S^{-N}[A]_{O'}$ are directly related to the position of the CPS O' with respect to the source of A.

The algorithm, presented by Stavrev (1997), is based on the results that: When the CPS coincides with the source singular point, the $S^{-N}[A]_{O'}$ of the anomaly field $F(A)$ becomes a zero at all observation points. The DST operator $S^{-N}[\cdot]_{O'}$ is linear, and therefore $S^{-N}[A + B]_{O'} = S^{-N}[A]_{O'} + S^{-N}[B]_{O'}$. When the background B is linear, $S^{-N}[B]_{O'}$ is linear, and then $S^{-N}[F]_{O'}$ of the measured field $F(P)$ also becomes linear. A linear regression could be applied to estimate the coordinates and structural index of the singular point, since the difference $S^{-N}[F]_{O'} - S^{-N}[B]_{O'}$ becomes equal to zero in theory, or reaches a minimum value in the real case when noise is present. Simultaneously, another linear regression is applied to obtain the parameters of the background. The dispersion of the difference between the DST of the measured field F and that of the background B is used to calculate the standard deviation of the solution, necessary afterwards for applying acceptance criteria. Stavrev (1997) offers the possibilities to use the algorithm with a prescribed structural index, or to estimate it. Here, we chose to take advantage of the option for unprescribed structural index and to apply the algorithm for processing of grid data.

After filtering the solutions, satisfying given acceptance criteria, we apply a two stage clustering technique to achieve better imaging of the depths and horizontal locations of the causative sources and to make a statistical analysis of the solutions. The first clustering is done on a micro scale in order to isolate the dispersed solutions. It is based on the rule that a point belongs to a cluster, if the distance between that point and all other points, belonging to the cluster, is smaller than a threshold value not bigger than one grid spacing. The second clustering stage combines the already focused solutions by the previous clustering in more general clusters and makes a fusion of the clusters. It identifies as belonging to the same cluster all clusters whose horizontal centre of gravity distance is less than the product of the maximum horizontal radius of confidence of all the clusters formed after the first clustering stage and a factor, chosen by the user. Finally, we apply a filtering that eliminates the clusters with less than a given number of points, since the clusters with small number of points are statistically not significant. The clustering on a macro scale allows obtaining of easily readable graphs of the solutions and facilitates their statistical analysis and tabular representation.

3. Program description

The method is divided into two main functions in order to allow the user to apply different acceptance criteria and clustering parameters to the same regression solutions, without having to recalculate the regression before every new parameter tuning trial. The first one, called AUTOEUL, finds optionally the first partial derivatives of the field and calculates and saves in a file all regression solutions and their dispersions (standard deviations), obtained through the use of the Euler deconvolution method. A second function, ACCEPTCL, takes this file as an input and applies acceptance criteria and solution clustering.

3.1. AUTOEUL function

The function implements Euler deconvolution with unprescribed structural index. It calculates optionally the derivatives of the field when the derivative matrices are not given as input. The field is approximated with bicubic splines for the calculation of the horizontal partial derivatives. The calculation of the vertical derivative is an important part of the data preparation for the deconvolution algorithm and should be paid special attention, since it amplifies the noise in the data. The vertical derivative is obtained in the frequency domain, using a standard filter. The procedure overcomes the problem with the edge effects by extending the grid 10% to the north and east with half a cosine function before the vertical derivative calculation. The extended area of the obtained derivative grid is then clipped back to the initial grid size.

This function takes as arguments:

(1) A matrix with the measured field data, with even number of rows and columns.
(2) Spacing of the data grid in x (north) direction.
(3) Spacing of the data grid in y (east) direction.
(4) Survey height in the same distance units as the grid spacings. The values are negative above ground level.
(5) Size of the window in x direction in grid points.
(6) Size of the window in y direction in grid points.
(7) A flag to activate y or deactivate n extension of the grid with 10% to the north and east with half a cosine function before the calculation of the field vertical derivative.
(8) Optional argument, the partial derivative of the field in x direction.
(9) Optional argument, the partial derivative of the field in y direction.

(10) Optional argument, the partial derivative of the field in z direction (vertically down).

The three additional arguments for the matrices with the partial derivatives can be used in the case of model studies or in case of partial derivatives, calculated with different methods from those, offered in the AUTOEUL function.

The only subjective choice the user should make at this stage is the window size. The latter can be determined experimentally with part of the data on the basis of the solution quality. The bigger the size of the window, the better focused the solution, but care should be taken not to include many interfering singular points in one window.

AUTOEUL calculates the relative to the estimated depth z_0 standard deviation σ_r of the obtained solutions σ, weighted by the estimated structural index, which will be compared with a threshold value τ in ACCEPTCL, i.e.

$$\sigma_r = N\frac{\sigma}{z_0}. \tag{6}$$

This is the same empirical criterion, as that suggested by Thompson (1982). All the solutions and some parameters, necessary for applying the acceptance criteria by the function ACCEPTCL, are saved in a Matlab file with the name EULER.MAT.

3.2. ACCEPTCL function

The function ACCEPTCL applies the acceptance criterion $\sigma_r < \tau$ on the obtained by AUTOEUL regression solutions and gives several options for their further processing. The first possible choice is to represent graphically the regression solutions satisfying the acceptance criterion and to save them in a file for further processing. The second possibility is to cluster the selected solutions for better imaging and statistical analysis. Following the latter option, the user can choose to eliminate the highly dispersed solutions and stop, or continue the clustering with another clustering parameter to obtain one final cluster for every singular point and accomplish a final statistical analysis and tabular representation of the results.

The ACCEPTCL function takes as arguments:

(1) The name of the Matlab file with all the regression solutions of the Euler deconvolution as a string.
(2) A number to indicate the clustering analysis level to be applied:
    0, no clustering;
    1, only the first stage micro scale clustering;
    2, both the first stage micro scale clustering and the second stage macro clustering, involving fusion of the obtained clusters as a result of the micro scale clustering.
(3) The threshold value τ for σ_r. This value must be adjusted by the interpreter. The solutions number decreases with decreasing τ.
(4) A fraction of the grid spacing ρ_{mic} to be used in the micro scale clustering. This parameter is used to multiply the grid spacing, the product of which would give the maximum horizontal distance, allowing two solutions to belong to the same cluster.
(5) A factor ρ_{mac} to be multiplied by the maximum horizontal radius of confidence of all the clusters to be used in the cluster fusion. This parameter is used to calculate the maximum distance, which allows for two clusters to be fused. We recommend that ρ_{mac} is equal or bigger than one.
(6) A scaling factor ρ_z to convert the depths to circles with radii proportional to the depths in the 2D graph representation of the clusters.
(7) Optional argument, the minimum number of points per cluster η. This parameter eliminates clusters and the associated to them points with less than η. When not included, the parameter has the default value $\eta = 5$.

Depending on the clustering analysis level, [ ] could be used as a place holder for the arguments that are not necessary.

In addition to the criterion that for a regression solution to be accepted as a singular point solution the expression σ_r should be less than a threshold value τ, ACCEPTCL uses a second criterion, according to which a solution is acceptable, if its estimated structural index $\hat{N}$ corresponds to a feasible one $0 < \hat{N} \leqslant 3$. All regression solutions, for which the estimated value of N are outside these limits, are ignored.

The first stage clustering algorithm is accelerated using a divide and conquer technique. The size of the batches is set as an internal parameter to 1500.

Furthermore, an additional clustering of the already obtained clusters is made possible. To reduce the number of clusters and to calculate the statistics for the solutions, an optional fusion of clusters algorithm was implemented, consisting of classifying in the same cluster all the points of the clusters whose horizontal centre of gravity distances are less than $\rho_{mac} r_h^{\max}$, where ρ_{mac} is a factor, chosen by the user, $r_h^{\max} = \max\left(\sqrt{c_x^2 + c_y^2}\right)$ is the maximum horizontal radius of confidence of all the clusters, and c_x and c_y are the half confidence intervals of the horizontal coordinates of each cluster's gravity centre.

After the last clustering stage an additional elimination of solutions is done. The eliminated solutions are those who form clusters with less than η points in a cluster. This is necessary to increase the statistical significance of the obtained Euler solutions. The default

value of η is set to 5 but since the issue of eliminating clusters with less than 5 points is not trivial, the user can optionally choose this limiting number depending on the sampling rate of the processed field. For each cluster the function makes a statistical analysis, calculating the mean value, the standard deviation and the confidence interval for the geometrical variables and the structural index, using a *t*-Student distribution with 95% certainty, based on the hypothesis that the solution follows a Gaussian distribution. In most of the cases (Reid et al., 1990; Stavrev, 1997) when the Euler deconvolution is used, the estimation of the quality of the solutions is done with a fixed tolerance and the certainty is estimated. Here, we apply the opposite approach, using a fixed certainty of 95% and estimating the confidence interval of the solution. The results from the statistical analysis are saved in an ASCII file with the fixed name STATDATA.TXT. The file has 10 columns, which save for every cluster the index of the cluster, the number of solutions classified in the cluster, the x horizontal position of its centre of gravity, the confidence interval for the x horizontal position, the y horizontal position of its centre of gravity, the confidence interval for the y horizontal position, the depth of the cluster centre of gravity, the confidence interval for the depth, the structural index and the confidence interval for the structural index.

In order to allow the user to make graphical representations and statistical analysis with other tools, all the accepted solutions, with their 3 coordinates and a structural index, are saved in an ASCII file with four columns with the fixed name SOLUDATA.TXT. The solutions for the parameters of the background are saved in a Matlab file BACKDATA.MAT.

For better understanding of the results, except for the files output, the function offers graphical representations. They include a graph of the horizontal location of the obtained solutions, with the depths represented by circles with centres at the horizontal projection of the source and a radius, proportional (the scaling factor ρ_z is chosen by the user) to the source depth. Other graphical representations are a 3D graph of the structural index values and a 3D graph, depicting the source locations.

If the clustering analysis is activated, the graphical representation of the tool includes additionally a 2D graph of the horizontal locations of the clusters and their depths as circles. The confidence interval for the depth is shown by two concentric circles around the circle, representing the average depth value. The confidence intervals for the horizontal coordinates are depicted by an ellipse with a centre, defined by their average values and axes, equal to the confidence intervals in the respective directions. The main axis of the ellipse helps to estimate the prevailing direction from which the solutions in a cluster were collected. Finally, a 2D graph of the clusters, represented by their indices, and a 2D graph, representing the solutions by their indices according to the classification to clusters, are generated.

4. Simple model application

The usage of the program tools is first illustrated on the total magnetic field ΔT of two isometric bodies (spheres) with added 5% Gaussian noise. The model field is shown in Fig. 1A. The partial derivatives were calculated by the AUTOEUL function, without extension of the grid. The algorithm was applied with a threshold value for the acceptance criterion $\tau = 0.0002$.

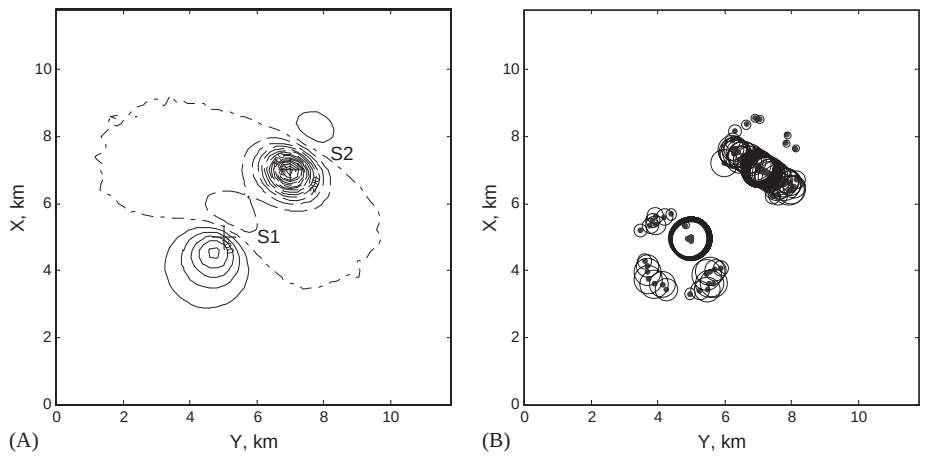

Fig. 1. (A) Model anomalous magnetic field ΔT, nT, of two isometric bodies with centre coordinates S1 (5,5,1.25) and S2 (7,7,1) with 5% added noise with Gaussian distribution. (B) Solutions for acceptance parameter $\tau = 0.0002$, without clustering analysis. Depth scaling parameter is $\rho_z = 0.5$.

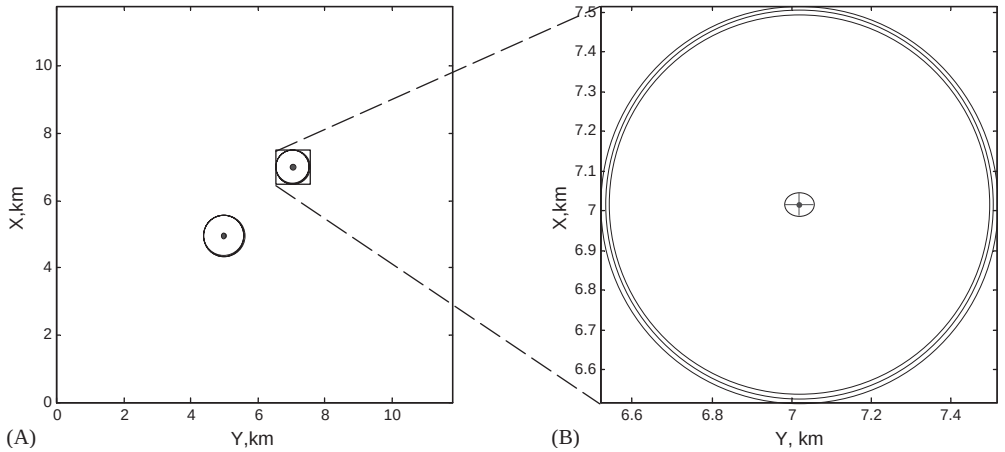

Fig. 2. (A) Solutions for model of two isometric bodies for acceptance parameter $\tau = 0.0002$, $\rho_{mic} = 0.01$ and $\rho_{mac} = 3$ after second clustering stage. (B) Graphical representation for confidence intervals for depth and horizontal coordinates of sources.

Table 1
Estimated (denoted with a hat) and true coordinates of singular points and their respective structural indices for 2 spheres example. Estimation is for a window of 15×15 points. Grid spacing is 0.2 km. Column n_{sol} shows obtained number of solutions for one singular point

Source	n_{sol}	$\hat{x}_0$ (km)	x_0 (km)	$\hat{y}_0$ (km)	y_0 (km)	$\hat{z}_0$ (km)	z_0 (km)	$\hat{N}$	N
Sphere S1	70	4.97 ± 0.02	5	4.97 ± 0.02	5	1.18 ± 0.07	1.25	2.79 ± 0.02	3
Sphere S2	86	7.02 ± 0.03	7	7.02 ± 0.04	7	0.98 ± 0.02	1	2.89 ± 0.01	3

Fig. 1B depicts the solution of the Euler deconvolution without clustering analysis. The effect of applying the two stage clustering is illustrated in Fig. 2A, where two clusters, corresponding to the two singular points, are obtained for a parameter of the first micro clustering $\rho_{mic} = 0.01$ and $\rho_{mac} = 3$ for the macro clustering. Fig. 2B shows a magnified view of the graphical representation of the clusters after the second clustering stage. The concentric circles show the confidence interval for the depth parameter around its average value, and the ellipsoid at the horizontal gravity centre of every cluster the 95% confidence interval for the two horizontal coordinates. The results of the statistical analysis for the final clusters are compared with the true parameter values in Table 1. The obtained coordinate and structural index solutions show acceptable deviations from the true values, taking into account the added amount of noise.

5. Complex model application

The tools were tested on a complex model total anomalous field example. The model consists of five causative bodies with ten singular points: two spheres (isometric bodies), one S1 at a depth of 2 km and another one S5 at 3 km, one sheet body (sill) S2, a dyke infinite in depth extent S3 and a horizontal rod S4. The bodies possess normal and reverse magnetisation and represent in a simple way the anomalous magnetic field of the Burgas region and the adjoining Black Sea shelf of Bulgaria (Fig. 8). The shallower sphere, the sheet and the horizontal rod are normally magnetised along the direction of the ambient field ($D_0 = 2.4^\circ$, $I_0 = 59^\circ$). The dyke and the deeper sphere are reversely magnetised. The total anomalous magnetic field ΔT of the model and the horizontal projections of the causative bodies, as well as their respective singular points, are shown in Fig. 3.

The true coordinates and structural indices of the singular points can be seen in Table 2, in the columns x_0, y_0, z_0 and N. The function AUTOEUL was applied with a window of 11×11 points, or 2.5×2.5 km. It used analytically calculated partial derivatives. The solutions were selected by ACCEPTCL, using a threshold value for the acceptance criterion $\tau = 0.0001$. The first clustering algorithm was applied with a parameter value $\rho_{mic} = 0.09$. The accepted solutions are focused but single fused clusters, corresponding to the respective singular points of the bodies, are still not formed. This is

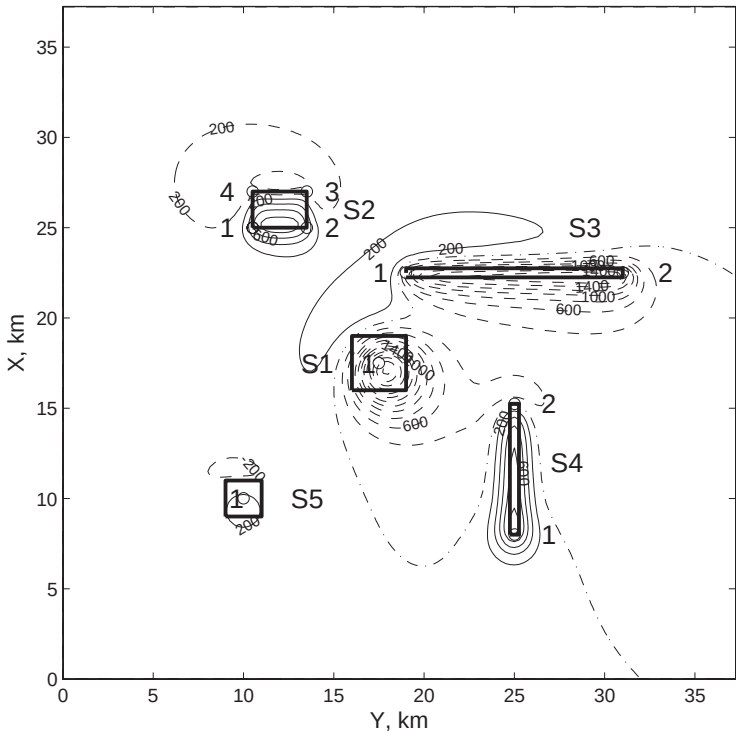

Fig. 3. Model anomalous magnetic field ΔT, nT, for complex model of five causative bodies: S1, S5 spheres (isometric bodies), S2 a sheet body (sill), S3 an infinitely deep dyke, and S4 a horizontal rod. Singular points of separate bodies are denoted with a circle and an index.

Table 2
Estimated (denoted with a hat) and true coordinates of singular points and their respective structural indices for 5 bodies example. Estimation is for a window of 11×11 points. Grid spacing is 0.25 km. Column *SP* denotes singular points of each source. Column n_{sol} shows obtained number of solutions for one singular point

Source	*SP*	n_{sol}	$\hat{x}_0$ (km)	x_0 (km)	$\hat{y}_0$ (km)	y_0 (km)	$\hat{z}_0$ (km)	z_0 (km)	$\hat{N}$	N
S1 sphere	1	170	17.49 ± 0.08	17.5	17.46 ± 0.07	17.5	2.95 ± 0.08	3	2.91 ± 0.15	3
S2 sill	1	10	24.97 ± 0.03	25	10.38 ± 0.01	10.5	1.08 ± 0.02	1	1.34 ± 0.04	1
	2	23	24.86 ± 0.14	25	13.63 ± 0.03	13.5	0.91 ± 0.1	1	0.85 ± 0.32	1
	3	25	27.12 ± 0.03	27	13.65 ± 0.04	13.5	0.72 ± 0.05	1	0.24 ± 0.13	1
	4	24	27.11 ± 0.05	27	10.33 ± 0.04	10.5	0.71 ± 0.06	1	0.21 ± 0.13	1
S3	1	343	22.6 ± 0.26	22.5	18.87 ± 0.92	19	0.81 ± 0.12	1	0.88 ± 0.64	1
Dyke	2	335	22.51 ± 0.11	22.5	31.25 ± 0.26	31	0.83 ± 0.06	1	1.06 ± 0.25	1
S4	1	542	7.76 ± 0.45	8	25.14 ± 0.53	25	1.54 ± 0.11	1.5	1.83 ± 0.51	2
Horiz. rod	2	30	15.34 ± 0.33	15.25	25.06 ± 0.43	25	1.45 ± 0.2	1.5	1.84 ± 0.83	2
S5 sphere	1	82	9.9 ± 0.11	10	9.97 ± 0.03	10	1.92 ± 0.08	2	2.77 ± 0.19	3

achieved after the second clustering stage with parameter $\rho_{mac} = 3$ which produces the solutions shown in Fig. 4 and the clusters in Fig. 5. Fig. 6 shows the positions of the depth solutions, while Fig. 7 presents the estimated structural indices in a 3D graph.

The mean values of the obtained solutions by the Euler deconvolution tool for the magnetic field of 5 bodies in Table 2 show good correspondence to the true parameters, except for the depth and structural index of singular points 3 and 4 of the sheet body S2, which is due to the strong interference and proximity of singular points 1-4 and 2-3 of S2. The small number of solutions for singular point 2 of the horizontal rod S4 is also due to interference from neighbouring singular points. The estimates of the structural index in Fig. 7 and Table 2 show wide bounds for singular points 1 and 2 of the

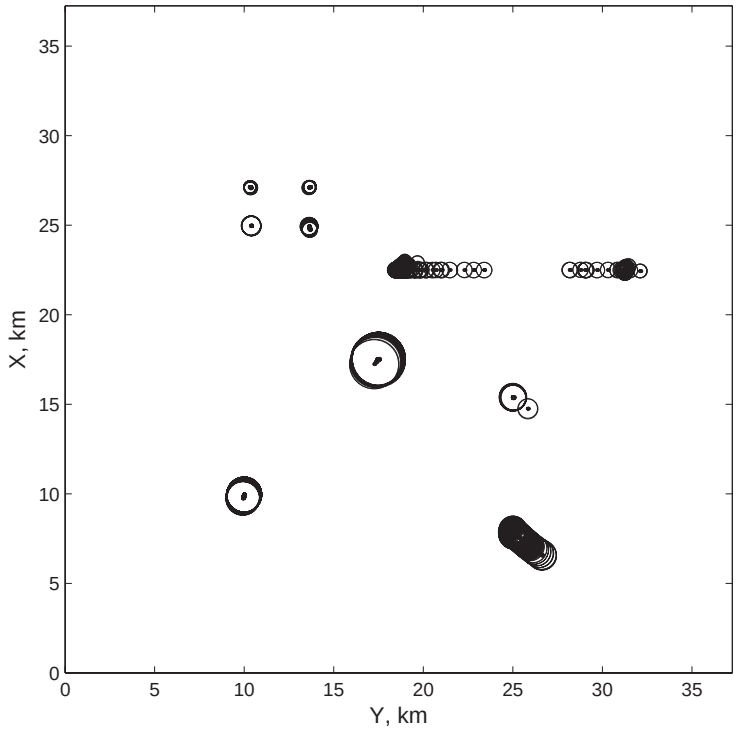

Fig. 4. Estimated locations of sources singular points for complex model of five magnetic bodies, clustering level 2, for ACCEPTCL arguments $\tau = 0.0001$ and $\rho_{mic} = 0.09$. Depth scaling parameter for graph representation of estimated depths is $\rho_z = 0.5$.

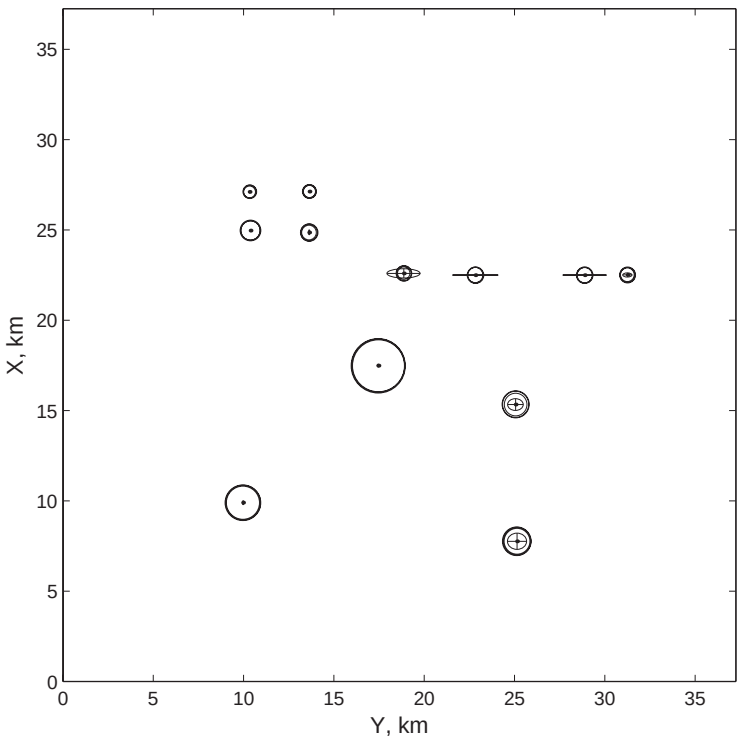

Fig. 5. Estimated locations of clusters of sources with confidence intervals for complex model of five magnetic bodies for ACCEPTCL arguments $\tau = 0.0001$, $\rho_{mic} = 0.09$ and $\rho_{mac} = 5$.

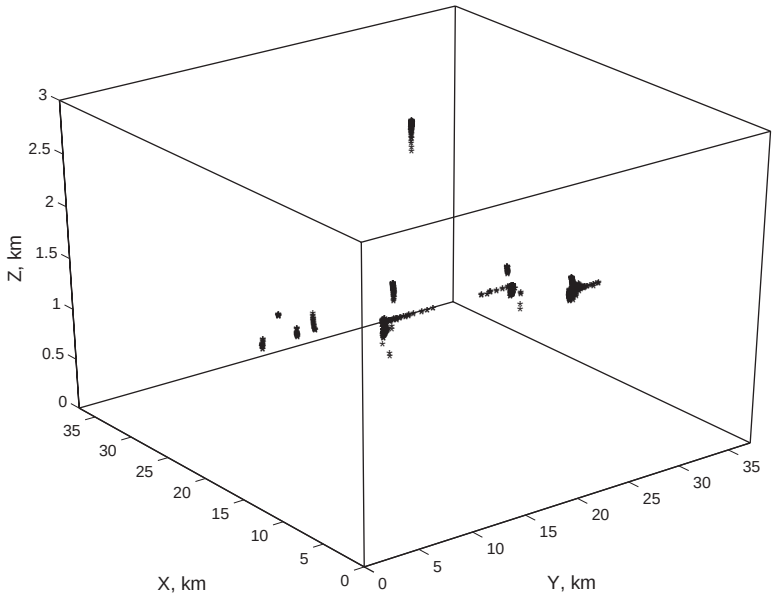

Fig. 6. 3D graph of estimated depths of sources singular points for complex model of five magnetic bodies.

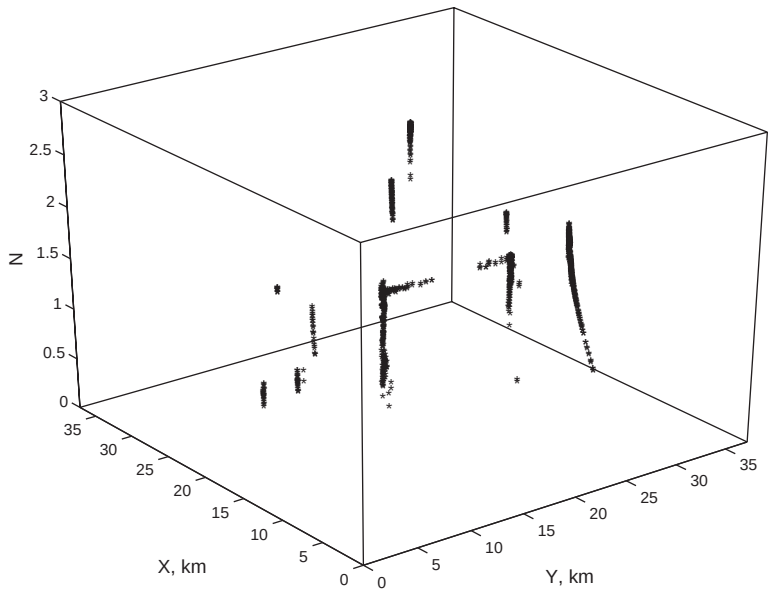

Fig. 7. 3D graph of estimated structural indices of sources singular points for complex model of five magnetic bodies.

horizontal rod and singular point 1 of the dyke. But this fact does not decrease the interpretational usefulness of the structural index mean value, compared to that of the other estimated parameters, which for these points are also high. The high confidence interval for correctly obtained mean values only reflects the effort of the algorithm, prepared to manage at most linear background, to cope with background with more complex model, due to the interference of the highly intense anomalies of the sphere S1, the dyke and the horizontal rod.

The estimation of the structural index provides valuable information on the geometry of the causative body. It helps to interpret correctly the obtained Euler depths, according to their associated structural index. Thus, we know that the Euler depth for singular point 1

of S1 should be interpreted as depth to the centre of an isometric body, while the Euler depths of singular points 1 and 2 of S1 should be regarded as depths to the upper top edges of one thin infinite in depth dyke.

6. Real data application

The Euler deconvolution tool was applied to real total field magnetic data ΔT from the Burgas region and the adjoining Black Sea shelf of Bulgaria (Fig. 8). The anomalous magnetic field is caused by the products of Upper Cretaceous magmatism in the area, and mainly by the Senonian andesite-basaltic and trachyandesite-trachybasaltic effusive associations and of the intrusive gabbro-monzosyenitic association (Dachev, 1988). The intense anomalies with positive and negative main extrema testify that the igneous rocks were formed during two phases of reversal of the magnetic field during the Senonian period. The Euler deconvolution algorithm was applied with a window of 21×21 grid points, for a grid spacing in both directions 0.5 km. The partial derivatives were calculated by AUTOEUL with extension of the field grid before calculating the vertical

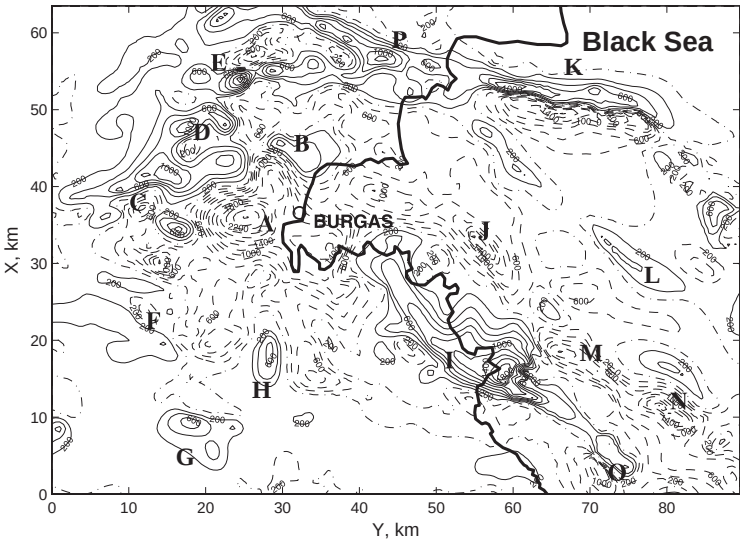

Fig. 8. Anomalous total magnetic field ΔT, nT, in Burgas region and adjoining Black Sea shelf, Bulgaria (after V. Pchelarov and L. Kerbelov). Grid spacing is 0.5 km in north and east directions.

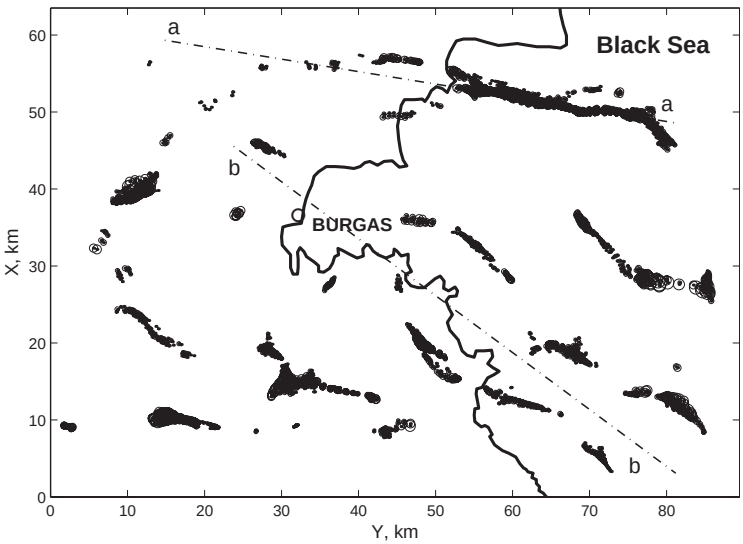

Fig. 9. Solutions of deconvolution algorithm for Burgas region and adjoining Black Sea shelf, Bulgaria, for $\tau = 0.0005$ and first clustering stage applied for $\rho_{mic} = 1$.

derivative. The acceptance criterion threshold value was chosen to be $\tau = 0.0005$. After the first clustering stage with parameter $\rho_{mic} = 1$, the solutions in Fig. 9 were obtained. The magnetic sources are located along two main axes. The first axis (a-a) has orientation WNW–ESE (100°). In the western part the geologic sources are shallow extrusive bodies, with the material supplied by nearby palaeovolcanos. To the east, in the Black Sea shelf, the anomalous magnetic field is caused by intrusive bodies along faults. The second line (b-b), about 20 km wide, has direction NW–SE at an angle 125°. Around this line, some intrusive bodies outcrop on the surface on the land. The sources of the most intense anomaly **K** in the Black Sea shelf, represented by clusters with indices 21, 23 and 28 (Fig. 11) show mean depth values of 0.8 km. The graph of the indices of the clusters, obtained after the second clustering stage, at the location of the average horizontal coordinates of the

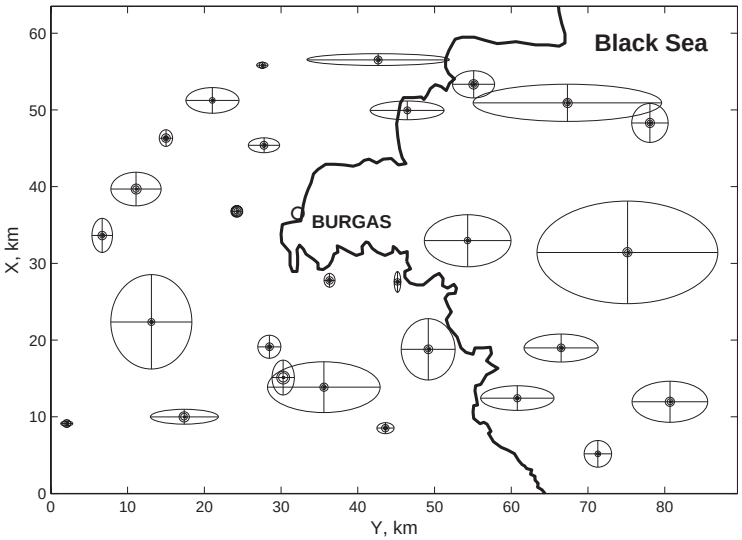

Fig. 10. Confidence intervals of horizontal position of centre of gravity of clusters with their depths, obtained with deconvolution algorithm for the Burgas region and adjoining Black Sea shelf, Bulgaria, for $\tau = 0.0005$ after second clustering stage, applied for $\rho_{mic} = 1$ and $\rho_{mac} = 1$. Depth scaling parameter is $\rho_z = 1$.

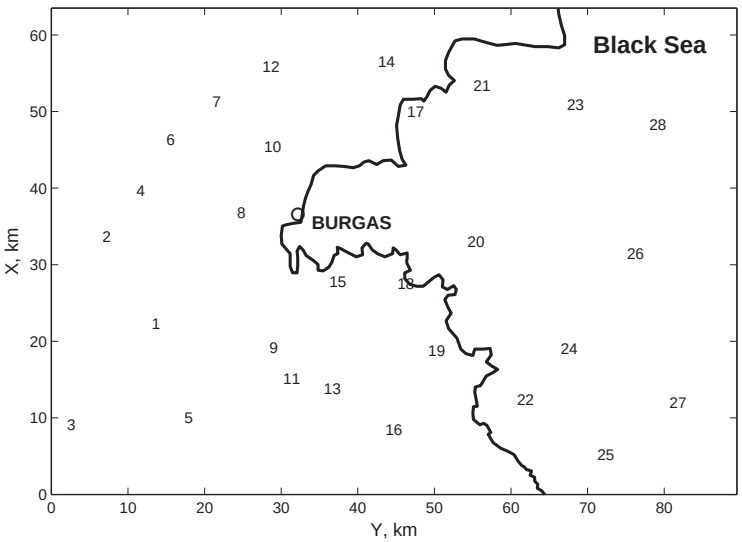

Fig. 11. Indices of final clusters for real magnetic data from Burgas region and adjoining Black Sea shelf, Bulgaria, after second clustering stage.

clusters (Fig. 11) helps in locating the spatial location of the solutions and the results from the statistical analysis of the corresponding cluster. These indices are the same as the cluster indices, saved in the STATDATA.TXT file. Most of the other linear sources in the Black Sea, represented by clusters 24, 26, 27, corresponding to anomalies **M**, **L** and **N**, show similar mean depths. The source for anomaly **G** on the ΔT map has an average depth 0.9 km, and that for the intense negative anomaly **A** 1.1 km. The sources along the line of the anomalies **C**, **D**, **E**, presented by clusters 2, 4, 6, 7 and 12, show depths between 0.3 and 0.8 km. Fig. 10 depicts the confidence intervals of the estimated singular points that show the main directions, from which the solutions were gathered after the second clustering stage to form a final fused cluster.

7. Conclusions

The developed tools for automatic interpretation of magnetic data are based on solving Euler's equation with unprescribed structural index. The implemented algorithm approximates the background in each moving window with a linear function, which reduces the error in the obtained solutions due to interference from neighbouring anomalies. It has the advantage of requiring as input only the measured field and avoids calculation of higher than first order field derivatives. The implemented two stage clustering technique eliminates diffused solutions, makes the imaging of the field sources more meaningful and facilitates direct statistical analysis of the solutions. The estimation of the structural index allows fast interpretation of magnetic anomalies of different interfering sources, and the association of a structural index value to each Euler depth gives more meaning to the interpretation of the depths. The usefulness of the tools and their different features were illustrated with two model magnetic data sets and real magnetic data from the Burgas region and the adjoining Black Sea shelf.

The tools, together with the simple and complex model data sets and the scripts to run the examples, are available at http://www.iamg.org/CGEditor/index.htm.

Acknowledgements

The authors would like to thank to Dr. A. Reid, Dr. M. Mushayandebvu and an anonymous reviewer for the comments and suggestions on the manuscript.

References

Barbosa, V.C.F., Silva, J.B.C., Medeiros, W.E., 1999. Stability analysis and improvement of structural index estimation in Euler deconvolution. Geophysics 64 (1), 48–60.

Dachev, H., 1988. Structure of the Earth Crust in Bulgaria. Tehnica, Sofia, 334pp. (In Bulgarian).

Hood, P.J., 1965. Gradient measurements in aeromagnetic surveying. Geophysics 30 (5), 891–902.

Hsu, S.K., 2002. Imaging magnetic sources using Euler's equation. Geophysical Prospecting 50 (1), 15–25.

Mushayandebvu, M.F., van Driel, P., Reid, A.B., Fairhead, J.D., 2001. Magnetic source parameters of two-dimensional structures using extended Euler deconvolution. Geophysics 66 (1), 814–823.

Reid, A.B., Allsop, J.M., Granser, H., Millett, A.J., Somerton, I.W., 1990. Magnetic interpretation in three dimensions using Euler deconvolution. Geophysics 55 (1), 80–91.

Ruddock, K.A., Slack, H.A., Breiner, S., 1966. Method for determining depth and falloff rate of subterranean magnetic disturbances utilising a plurality of magnetometers. US Patent 3,263,161.

Stavrev, P.Y., 1997. Euler deconvolution using differential similarity transformations of gravity or magnetic anomalies. Geophysical Prospecting 45 (2), 207–246.

Thompson, D.T., 1982. EULDPH: A new technique for making computer-assisted depth estimates from magnetic data. Geophysics 47 (1), 31–37.